J. Fluid Mech. (1982), *vol.* 115, *pp.* 427–442
Printed in Great Britain

Closed-cavity laminar flows at moderate Reynolds numbers

By J. F. BRADY† AND A. ACRIVOS
Department of Chemical Engineering, Stanford University, Stanford, CA 94305

(Received 13 October 1980)

The paradox reported by Brady & Acrivos (1981) of the non-existence of similarity solutions in the Reynolds-number range $10{\cdot}25 < R < 147$ for the flow in a tube with an accelerated surface velocity is resolved. It is shown that the source of the difficulty lies in the assumption that the tube is infinite in extent. For a finite tube, it is demonstrated that the presence of the closed end, even though far removed from the origin, affects in a fundamental way the structure of the flow throughout the entire tube. The change in the flow structure that occurs in a finite tube at $R = 10{\cdot}25$ is caused by the fluid which is returning from the downstream end; it is shown further that the problem of determining the motion in a long finite tube is equivalent to that of selecting the initial condition for the boundary-layer equations that properly takes into account the presence of the reverse flow. By applying a method originally developed by Klemp & Acrivos (1976) for selecting this condition, the flow in a finite tube is determined numerically for Reynolds numbers up to 70. In addition, it is shown that the same change in structure brought about by the returning fluid occurs in a finite two-dimensional channel at $R = 57$, even though the corresponding similarity solutions exist for all values of R. The results suggest that similarity solutions should be viewed with caution because they may not represent a real flow once a critical Reynolds number is exceeded.

1. Introduction

In a previous paper (Brady & Acrivos 1981), hereinafter referred to as I, we presented an exact solution to the steady Navier–Stokes equations for the flow in a semi-infinite channel or tube which is driven by an accelerating surface velocity (cf. figure 1 in I). For the two-dimensional case, a well-behaved set of solutions that evolve continuously with the Reynolds number R was found to exist for all $0 \leqslant R < \infty$. This is in contrast to the corresponding axisymmetric case without swirl where no solutions exist within the range $10{\cdot}25 < R < 147$. (As discussed in I, the axisymmetric solutions with swirl do not evolve from $R = 0$, nor do they bifurcate from those without swirl at any finite value of R; hence they will not be considered in this paper.) The presence of this gap in the axisymmetric solutions raises an important question regarding the structure of the flow in a 'real tube' as the Reynolds number is increased from zero to 10·25, and then beyond. One of the aims of this paper is to answer this question.

We shall show in what follows that the source of our difficulties lies in the assumption that the tube is semi-infinite in extent. Of course, in any real physical problem, the tube's length must be finite, and we shall see that the existence of a closed end, even

† Present address: Department of Chemical Engineering, Massachusetts Institute of Technology, Cambridge, Massachusetts 02139.

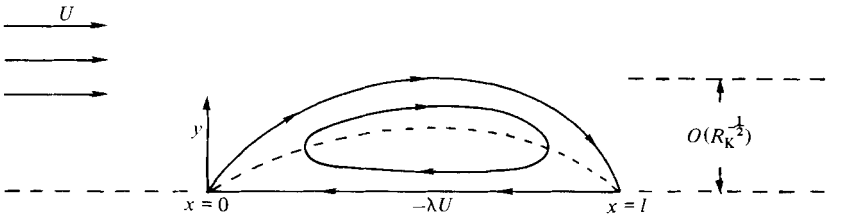

FIGURE 1. Region of closed streamline flow, adjacent to a flat plate, whose surface velocity moves in a direction opposite to that of the free stream; $R_K = Ul/\nu$ (after Klemp & Acrivos 1976).

though it may be far removed from the origin, affects, in a very fundamental way, the structure of the flow throughout the entire tube if R is sufficiently large.

At first, the sudden disappearance of a similarity solution for $R > 10{\cdot}25$ is puzzling because, even in a finite tube, one would expect such a solution to apply over most of the length of a very long tube. And, in fact, we shall show that the similarity solution does indeed accurately describe the flow in a finite tube over most of its length provided R is small. As R is increased, however, we shall see that the range of validity of the similarity solution continuously decreases, until at $R = 10{\cdot}25$ it has shrunk to zero. In addition, we shall show that, at this critical value of R, the flow in a finite tube undergoes a fundamental change in structure which no longer bears any resemblance to that given by the similarity solution.

This change in the flow pattern which occurs in a finite tube is brought about by the fluid returning from the downstream end. We recall from the similarity solution (cf. equation (2.3) in I) that the longitudinal velocity of this returning fluid, being proportional to the streamwise co-ordinate x, must vanish by the time it reaches the origin. In a closed tube, however, if the Reynolds number becomes too large, the strength of the viscous forces, which play the dominant role in slowing down the returning fluid, will be insufficient to overcome the momentum of this fluid before it reaches the origin $x = 0$. Of course, in a closed region of flow, the pressure is simply set up so as to conserve mass and cannot act to retard the returning fluid. Hence, once a critical value of R is exceeded, this returning fluid will no longer have a vanishingly small axial velocity as $x \to 0$. Rather, it will 'collide' with its mirror image from negative x, forming, as we shall show, an inviscid region of flow near $x = 0$ in which the similarity solution no longer applies. In fact, there is a close analogy between the present problem and that studied by Klemp & Acrivos (1972, 1976) for the high-Reynolds-number laminar flow over a finite-length flat plate whose surface is moving in a direction opposite to that of the free stream. To aid in our presentation, we shall first review the principal features of the solution developed by these authors.

As illustrated in figure 1, the negative velocity of the plate's surface sets up a region of closed streamline flow adjacent to the plate that remains confined within the boundary layer if the Reynolds number is sufficiently large. Near the leading edge of the plate, a similarity transformation reduces the boundary-layer equations to the Blasius equation, and, in a manner analogous to the results of I, solutions to this equation cease to exist once the ratio of the surface speed to that of the free stream, called λ by Klemp & Acrivos, reaches 0·3541. (The analogy is actually quite strong because, by scaling x with R in the similarity solution of I (cf. (2.3) in I), the Reynolds number can be removed from the governing equation and transferred to one of the boundary conditions at the moving surface.) Furthermore, Klemp & Acrivos (1972)

found that the similarity solution accurately described the flow over most of the length of the plate provided λ was less than 0·2, but that, as $\lambda \to 0{\cdot}3541$, the region of validity of this similarity solution had shrunk to a single point. These authors then postulated that, at this critical value of λ, an inviscid region of flow forms at the leading edge of the plate whose lateral and vertical dimensions are $O(R_K^{-\frac{1}{2}})$, where $R_K \equiv Ul/\nu$ is the Reynolds number in their problem. In this inviscid region, the fluid dragged along by the moving surface of the plate collides with the main stream and is turned around to flow back downstream, still, however, remaining within an $O(R_K^{-\frac{1}{2}})$ distance of the surface. Thus, the boundary-layer equations still govern the flow near the plate, but the similarity solution no longer describes the motion near the leading edge. In this way, Klemp & Acrivos (1976) were able to develop solutions for all values of λ.

We shall now show that, by postulating the presence near $x = 0$ of a collision region analogous to that described by Klemp & Acrivos (1976), solutions for the accelerating-tube-flow problem can be obtained for values of R in excess of 10·25. In § 2 we shall reformulate the problem described in I for a tube of finite length, and shall show how to take into account the presence of an inviscid collision region when setting up the boundary condition at $x = 0$. In § 3 we shall present the resulting numerical solutions to the appropriate equations for the accelerating-tube-flow problem for Reynolds numbers up to 70. Since this concept of allowing for the presence of a collision region at the origin is not restricted to the present problem (nor to that considered by Klemp & Acrivos), we shall extend our analysis in § 4 to other types of closed-cavity flows. In that section we shall also discuss the relation between similarity solutions and the real flows that they are meant to represent, and shall offer the suggestion that, in boundary-layer problems with reverse flow, the existence of an inviscid collision region may be the rule rather than the exception.

Thus, the aim of this paper is much broader than merely providing numerical solutions to a specific problem in that it also contains the application of a mathematically consistent scheme for integrating the boundary-layer equations in the presence of reverse flow that, although available in the literature, does not appear to have received much attention. Moreover, since it is possible here to make a comparison between a 'real' flow and that given by a similarity solution, we are able to examine the important question of the relationship between similarity solutions and the real flows that they are meant to represent, a relationship which, as we shall see, is not necessarily a simple one.

2. The flow in a tube of finite length

In reformulating the problem of I for a finite-length closed tube or cavity, we shall not specify any detailed boundary conditions at the end of the tube, but simply require that the tube be closed. We shall denote the length of the cavity by L and its radius by a, with $a/L \ll 1$ for long slender cavities. We shall denote the cavity surface by $r = ah(x)$, where $h(x)$ is an $O(1)$ function of x which varies on a length scale L. At the surface, the axial velocity will be $u = Ex$ (cf. figure 1 in I), while the radial component v will satisfy the kinematic conditions of zero normal flux across the surface; thus $v = uah_x = Eaxh_x$, where $h_x = dh/dx$ (see figure 2). Also, the centre line will be a line of symmetry, $\partial u/\partial r = v = 0$ at $r = 0$, and the flow is to be antisymmetric about the origin.

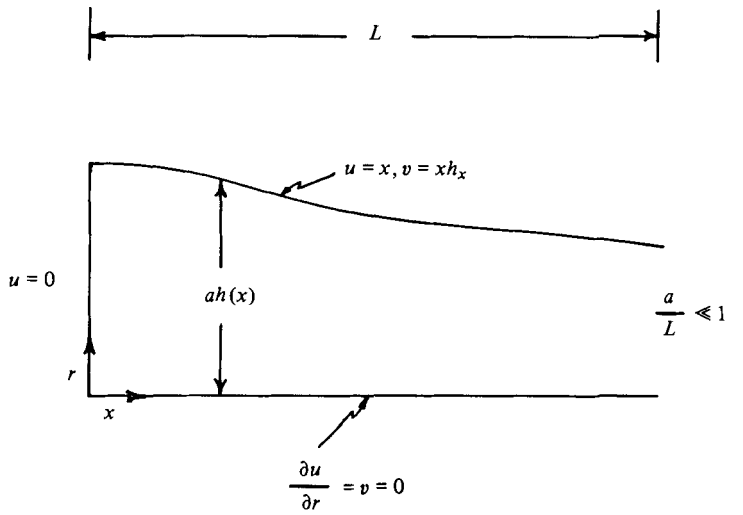

FIGURE 2. Schematic diagram for the flow in a long slender finite cavity with an accelerating surface velocity.

Since the problem now contains two length scales, L and a, we have a choice as to how to scale the equations of motion. The natural choice is to scale r and v with a and Ea respectively, and the axial co-ordinate and velocity with L and EL. If the pressure is scaled with $\mu E(L/a)^2$, then the equations of motion in dimensionless form become, for long slender cavities,

$$R\left\{u\frac{\partial u}{\partial x}+v\frac{\partial y}{\partial r}\right\}+\frac{\partial p}{\partial x}=\frac{1}{r}\frac{\partial}{\partial r}\left(r\frac{\partial u}{\partial r}\right)+O\left[\left(\frac{a}{L}\right)^2\right], \tag{2.1}$$

$$\frac{\partial p}{\partial r}=O\left[\left(\frac{a}{L}\right)^2\right], \tag{2.2}$$

where $R \equiv \rho Ea^2/\mu$ is the Reynolds number. The boundary conditions for (2.1) are

$$u = x, \quad v = xh_x \quad \text{at} \quad r = h(x); \tag{2.3a,b}$$

$$\frac{\partial u}{\partial r} = v = 0 \quad \text{at} \quad r = 0. \tag{2.4a,b}$$

As $a/L \to 0$, (2.1) and the equation of continuity are seen to be the axisymmetric forms of the boundary-layer equations, with the exception that the transverse co-ordinate r is $O(1)$ and the Reynolds number appears as a parameter in the equations. Here, a/L is the small parameter rather than the reciprocal of the Reynolds number as is normally the case in boundary-layer theory. Furthermore, we should note that, since the characteristic axial velocity is $O(EL)$, neither R nor the equations contain L explicitly; thus, so long as $(a/L) \ll 1$, the absolute scale of L is immaterial.

If we assume that (2.1)–(2.4) apply for all x, it is clear that the similarity solution $u = xf'(r)/r$, developed in I, will represent the first term in a Taylor-series expansion of u about the origin for any analytic function $h(x)$. Hence we would expect the similarity solution to be valid near $x = 0$, in much the same way that the Blasius equation was expected to describe the flow near the leading edge of the flat plate problem considered by Klemp & Acrivos (1976). It should be obvious, however, that

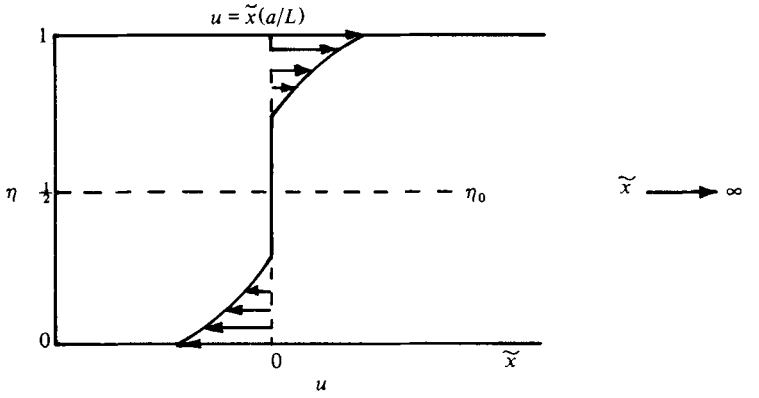

FIGURE 3. Structure of the longitudinal velocity profile in the overlap domain between the inner and outer regions when $\eta_0 = \frac{1}{2}$. (Note that $(\partial u/\partial \eta)_{\eta=0} \neq 0$.)

(2.1) is not necessarily valid within an $O(a/L)$ region near $x = 0$ because, when x is small, it should be scaled with a as opposed to L. In other words, (2.1) should be viewed as applying to the flow in an 'outer' region whose solution must match with the solution to an equation that applies near the origin. We see then, that the proper initial condition for the boundary-layer equation (2.1) is one of matching as $x \to 0$ with a solution which is valid in an 'inner' region.

The flow in this inner region can have one of two structures depending on the magnitude of the returning velocity. If this velocity vanishes as $x \to 0$, then (2.1) and the similarity solution will continue to apply up to $x = 0$, i.e. the inner region will be absent, and $u = 0$ is the appropriate initial condition. If, however, the dimensionless velocity of the returning fluid does not vanish, but instead remains $O(1)$ – i.e. $O(EL)$ in *dimensional* units – then the effective Reynolds number within this inner region will be $(L/a)\,R$, which, for any non-zero R, is arbitrarily large as $a/L \to 0$. Consequently, in this later case, the inner region will be inviscid, and the form of u in (2.1) as $x \to 0$ must be chosen to be consistent with the motion in this inviscid inner (or collision) region. We should also note that the two different inner regions will produce cavity flows with a fundamentally different mathematical structure as $x \to 0$.

In general, the determination of the complete flow field in the inviscid collision region will require considerable effort. Fortunately, however, this is not necessary because the only role of this region is to supply an initial condition for the boundary-layer equation (2.1); a condition that can be obtained quite simply from matching. Specifically, in an axisymmetric inviscid flow, the vorticity divided by r is constant along streamlines and thus

$$4\frac{\partial^2\psi}{\partial\eta^2} + \frac{1}{\eta}\frac{\partial^2\psi}{\partial\tilde{x}^2} = -F(\psi), \tag{2.5}$$

where $F(\psi) = \omega/r$, ω being the vorticity, $\eta = r^2$, $\tilde{x} = xL/a$, and ψ is the stream function, i.e. $u = 2\,\partial\psi/\partial\eta$ and $v = -\eta^{-\frac{1}{2}}\,\partial\psi/\partial\tilde{x}$. Since v is of a different order of magnitude in the inner and outer regions, matching between the two regions requires that $\partial\psi/\partial\tilde{x} \to 0$ as $\tilde{x} \to \infty$, i.e. that all streamlines must become parallel to the axis. If now we consider a point η_0 at which $u = 0$, then from (2.5) we see that, as $\tilde{x} \to \infty$, u must be antisymmetric about η_0, and, since mass must be conserved at any cross-section, $\eta_0 \leqslant \frac{1}{2}$.

Although this matching between the inner and outer regions does not determine a unique initial condition, the choice $\eta_0 = \frac{1}{2}$ leads to the most realistic initial velocity profile. As illustrated in figure 3, when $\eta_0 = \frac{1}{2}$, the fluid that returns along the axis is deflected up to the surface and then flows back downstream just beneath the wall of the cavity. On the other hand, if η_0 were less than $\frac{1}{2}$, this same fluid would return downstream at $2\eta_0$, thereby creating a region of stagnant fluid adjacent to the surface, which is rather unphysical. Hence, we shall assume that $\eta_0 = \frac{1}{2}$ and that the axial velocity at the edge of the inner region has the form depicted in figure 3. (Incidentally, numerical solutions computed with $\eta_0 < \frac{1}{2}$ were essentially identical to those with $\eta_0 = \frac{1}{2}$, except, for $\eta > \eta_0$, for the first one or two grid points near $x = 0$.) Thus, if we let u denote the axial component of velocity for $0 \leqslant \eta \leqslant \frac{1}{2}$ in the overlap domain between the inner and outer regions, then the solution within the inviscid collision region requires that the initial condition for (2.1) be

$$u(\eta) = -u(1-\eta), \quad 0 \leqslant \eta \leqslant \tfrac{1}{2}, \quad \text{at} \quad x = 0. \tag{2.6}$$

Equation (2.6) expresses the fact that the fluid which is returning from downstream, $u \leqslant 0$, $0 \leqslant \eta \leqslant \frac{1}{2}$, collides and reappears $u \geqslant 0$, $\frac{1}{2} \leqslant \eta \leqslant 1$, in such a way so that ω/r is conserved along streamlines. This conservation of vorticity allows us to understand the appearance of a collision region in a different way. The fluid returning from the end of the cavity will, in general, have vorticity which can only be lost through the action of viscosity, i.e. by diffusion. As the Reynolds number increases, the rate of diffusion of vorticity decreases, and, once a critical Reynolds number is exceeded, the returning fluid will not be able to dissipate its vorticity by the time it has reached the origin.

Having shown how the structure of the flow near the origin in a tube of finite length changes with Reynolds number, we can now use this analysis to construct solutions for R exceeding 10·25. In place of the similarity solution, (2.6) will serve as the initial condition for the boundary-layer equations when R is greater than 10·25. To determine u at $x = 0$ for $0 \leqslant \eta \leqslant \frac{1}{2}$, we can extrapolate the velocity in the outer region backwards as $x \to 0$. In this way the returning fluid will determine the initial condition and hence affect the motion throughout the entire cavity.

3. Numerical solution for the accelerating cavity flow

To obtain a solution for all values of the Reynolds number we need to solve for the flow in a finite cavity, which, unfortunately, can only be done numerically. This requires that we specify completely the geometry of the cavity. As we shall show at the end of this section, all slowly varying cavity shapes will give rise to a collision region at $R = 10{\cdot}25$, but the shape $h(x) = 1 - x^2$, $0 \leqslant x \leqslant 1$, where x has been scaled with L as in (2.1), will be used for the numerical calculations. It is also convenient to transform the domain into a square by defining $\eta = r^2/h^2(x)$ and rewriting (2.1), along with the equation of continuity, as

$$Rh^2\left\{\frac{\partial u}{\partial t} + u\frac{\partial u}{\partial x} + (V - 2\eta h_x u)\frac{1}{h}\frac{\partial u}{\partial \eta}\right\} + h^2\frac{dp}{dx} = 4\frac{\partial}{\partial \eta}\left(\eta\frac{\partial u}{\partial \eta}\right), \tag{3.1}$$

$$\frac{\partial V}{\partial \eta} + h\frac{\partial u}{\partial x} - 2\eta h_x\frac{\partial u}{\partial \eta} = 0, \tag{3.2}$$

where $V = 2\eta^{\frac{1}{2}}v$ and the time derivative of u has been retained in the inertial terms. The boundary conditions, which are now located at fixed positions, are

$$u = x, \quad V = 2xh_x \quad \text{at} \quad \eta = 1, \tag{3.3}$$

$$\lim_{\eta\to 0} \eta^{\frac{1}{2}} \frac{\partial u}{\partial \eta} = 0, \quad \text{and} \quad V = 0 \quad \text{at} \quad \eta = 0. \tag{3.4a,b}$$

The motivation for selecting this form of $h(x)$ comes from the problem of drop breakup (to be discussed in a subsequent paper (Brady & Acrivos 1982)) where flows inside cavities of this shape are required. This and similar choices for h, however, also help to simplify the numerical analysis because these shapes remain slender everywhere up to the end of the cavity, thereby enabling us to focus attention on the flow near $x = 0$. (Any shape which abruptly closes at $x = 1$, such as $h(x) = 1$, $0 \leqslant x < 1$ and $h(1) = 0$, would give rise to a 'singular' region near the end within which the fluid would be turned around.) In fact, from (3.1) we see that, when $h = 1 - x^2$, the effective Reynolds number $Rh^2(x)$ varies over the length of the cavity and vanishes at $x = 1$. Hence the flow near the end will be required to conform to that given by the zero-Reynolds-number solution, i.e.

$$u = 2x(\eta - \tfrac{1}{2}), \tag{3.5}$$

$$h^2 \frac{dp}{dx} = 8x \quad \text{as} \quad x \to 1. \tag{3.6}$$

We should also note that the zero-Reynolds-number solution expressed in terms of η is of the similarity form $-u/x =$ a function of the transverse co-ordinate $-$ over the entire length of the cavity. It is unusual of course to specify the downstream boundary condition for a parabolic equation, but it should be noted that, since the returning velocity at $x = 0$ is *a priori* unknown, the initial condition given by (2.6) is insufficient by itself to determine uniquely the flow throughout the cavity. In effect, (2.6) serves as a consistency condition between the collision region and the motion in the remainder of the cavity. On the other hand, (3.5) determines how the fluid is to return from the downstream end, and therefore the problem can be viewed as how to choose the initial condition, given R and $h(x)$, so that the fluid returning from downstream satisfies (3.5).

To obtain the numerical, finite-difference, solution for the flow inside the cavity, (3.1) was solved dynamically in time until a steady state was achieved throughout the entire flow field. Space-centred differences were used in both the η- and x-directions, and (3.1) was stepped forward in time explicitly in the x-direction but implicitly in the η-direction. The relatively large number of grid points needed in the η-direction, coupled with the fact that solutions for a wide range of R were computed, would have placed too severe a restriction on the time-step size if a fully explicit scheme had been used. The implicit formulation in η leads to a tri-diagonal system of linear equations, which can be solved quickly, thereby achieving a net gain in computational speed.

In operator notation the finite-difference equations are

$$Rh^2\left\{\delta_t u + u\delta_{2x}u + (V - 2\eta h_x u)\frac{1}{h}\delta_{2\eta}\bar{u}^t\right\} + h^2\frac{dp}{dx} = 4\{\delta_{\eta\eta}(\overline{\eta u})^t - \delta_{2\eta}\bar{u}^t\}, \tag{3.7}$$

$$\delta_\eta V + h\delta_{2x}\bar{u}^\eta - 2\eta h_x \delta_\eta u = 0. \tag{3.8}$$

Here, the difference operators are defined by

$$\left.\begin{aligned} \delta_\xi \phi(\xi) &= (\Delta\xi)^{-1}\{\phi(\xi+\Delta\xi)-\phi(\xi)\}, \\ \delta_{2\xi}\phi(\xi) &= (2\Delta\xi)^{-1}\{\phi(\xi+\Delta\xi)-\phi(\xi-\Delta\xi)\}, \\ \delta_{\xi\xi}\phi(\xi) &= (\Delta\xi)^{-2}\{\phi(\xi+\Delta\xi)-2\phi(\xi)+\phi(\xi-\Delta\xi)\}, \\ \overline{\phi}^{\xi} &= \tfrac{1}{2}\{\phi(\xi+\Delta\xi)+\phi(\xi)\}, \end{aligned}\right\} \tag{3.9}$$

where ϕ is the appropriate dependent variable and ξ the independent variable. Also, since we are only interested in steady solutions, the function $h^2(x)$ multiplying the time derivative can be set equal to unity, which enhances the stability of the system without affecting the final solution. This is equivalent to replacing Δt in (3.7) by $h^2\Delta t$ and introduces an error into the effective time-step size near the end, which, since the Reynolds number is essentially zero there, has little effect on the dynamical calculations.

To complete the numerical scheme, we must devise a method for computing the pressure, which is unknown and must be found as part of the solution. In closed-cavity flows, the pressure is set up to conserve mass, and hence the zero-flux requirement

$$\int_0^1 u(x,\eta)\,d\eta = 0 \tag{3.10}$$

will furnish us with the additional equation needed to find dp/dx. Since the pressure gradient is unknown at $t+\Delta t$ (with, as mentioned above, the term h^2 multiplying the time derivative set equal to unity), we first calculate from the finite-difference equation (3.7)

$$\hat{u} \equiv u + \frac{1}{R}\Delta t\, h^2 \frac{dp}{dx},$$

which will not, in general, satisfy (3.10); thus

$$\frac{1}{R}h^2\Delta t\frac{dp}{dx} = \int_0^1 \hat{u}\,d\eta,$$

which when subtracted from $\hat{u}$ determines u at $t+\Delta t$. Hence, the pressure gradient evolves in time in such a way that the net flux of fluid across each axial station remains zero.

At time $t = 0$ the flow field was set equal to that given either by the zero-Reynolds-number solution, or by a previously computed solution at a different R. Because of the implicit representation in η, all the u-values in a given column had to be determined simultaneously; hence, a time step was taken by sweeping through the flow field in the positive x-direction and solving at each value of x a tri-diagonal matrix for u. The initial condition (2.6) was used at $x = 0$ while, at $x = 1$, the velocity field u was required to satisfy (3.5). (We should note that (3.5) gives a valid description of the flow near $x = 1$ provided Δx is sufficiently small so that the local Reynolds number $R\Delta x$ is also small.) At the end of each time step a new initial condition at $x = 0$ was computed in the manner described below, and the procedure was repeated until a steady state was attained throughout the entire domain.

To determine the initial condition in x at the beginning of each time step, we started at $\eta = 0$ and simply extrapolated u backwards from the next two grid points downstream, increasing η until $\eta = \frac{1}{2}$. Although a linear extrapolation produced accurate results for most of the calculations, some care was needed in determining the proper

form for the extrapolation. Since, at $x = 0$, $u(\eta = 0)$ was generally non-zero, and since the solution in the inviscid collision region requires that $u(\eta = 1) = -u(\eta = 0)$, the velocity at $x = 0$ was discontinuous at $\eta = 1$ (cf. (3.3), according to which $u(\eta = 1) = 0$). This discontinuity in turn implies that the boundary-layer equations will have a singularity at $x = 0$ analogous to that occurring in the entry flow in a pipe (Van Dyke 1970). As a result, the expression for u as $x \to 0$ takes on the form $u \sim u_0(\eta) + x^{\frac{1}{2}}u_1(\eta)$, which in turn implies that both dp/dx and the inertial terms will become $O(x^{-\frac{1}{2}})$ as $x \to 0$. We see then, that the proper form for the extrapolation should be linear in $x^{\frac{1}{2}}$ rather than in x.

In order for both the flow field and the initial condition to evolve together in time, at the beginning of each time step the velocity for $\eta \leqslant \frac{1}{2}$ was extrapolated backwards to determine the initial condition. If all the extrapolated velocities were zero, then the initial condition is $u = 0$ for all η, which simply corresponds to the similarity solution at $x = 0$. (A positive u could result if the mesh size was too large, and in this case u was set equal to zero.) Thus, by extrapolation, both the structure of the collision region, and the transition from the similarity solution to the inviscid collision region evolved in time. This proved to be very convenient and is actually quite important because, although it is clear from the previous discussion that an inviscid collision region must be present when $R > 10{\cdot}25$, there is no reason why the collision region cannot appear when R is less than 10·25. Rather than having to make this decision at the outset, it was made dynamically in time so as to be completely consistent with the equations of motion.

To properly resolve the singularity in (3.1) at $x = 0$ a small mesh size is needed in both the η- and x-directions. Rather than using an excessively large grid, the axial co-ordinate was exponentially stretched by defining

$$x = \frac{e^{\alpha z} - 1}{e^{\alpha} - 1} \quad (0 \leqslant z \leqslant 1),$$

where α is a positive constant; in so doing, a large number of grid points were placed near the origin. With $\alpha = 3$ and 26 grid points for z we could reduce Δx to $6{\cdot}29 \times 10^{-3}$ at $x = 0$ without losing accuracy near $x = 1$ ($\Delta x = 0{\cdot}126$ at $x = 1$). Very good accuracy was achieved up to a Reynolds number of 70 – the largest for which a solution was computed – by using 91 grid points in the η-direction. A time-step size was used which satisfied the linear stability requirement in the axial direction, i.e. $\Delta t < \Delta x/u \simeq \Delta x$, which, even for this nonlinear problem, was found to be extremely accurate. The calculations were terminated when the maximum absolute error in the pressure gradient between time steps was less than 9×10^{-7} everywhere. (The pressure was found to converge more slowly than the velocity field.) Depending on the initial flow, this required a dimensionless time of between 3 and 5.

The results of the numerical computations for the flow in a finite closed cavity are shown in figure 4, where the pressure gradient $h^2 dp/dx$ is plotted as a function of x for various values of the Reynolds number. The dashed curves shown in figure 4 represent the pressure distributions computed from the similarity solutions at $R = 1$, 5 and 10·25 (cf. I). The form of the pressure gradients show very clearly that the similarity solution represents the flow in a finite cavity quite accurately (the velocity profiles are also in close agreement) when the Reynolds number is less than unity. As R increases, however, the flow predicted by the similarity solution and that in a finite tube coincide

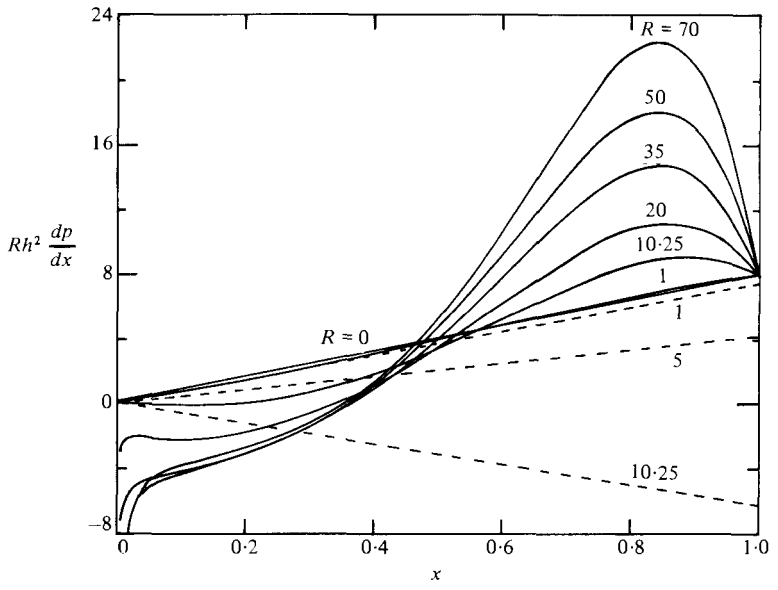

FIGURE 4. Pressure-gradient profiles for the flow in a finite axisymmetric cavity ($h(x) = 1-x^2$) at $R = 0, 1, 10{\cdot}25, 20, 35, 50, 70$. The dashed curves correspond to the pressure-gradient profiles predicted by the similarity solution at $R = 1, 5, 10{\cdot}25$.

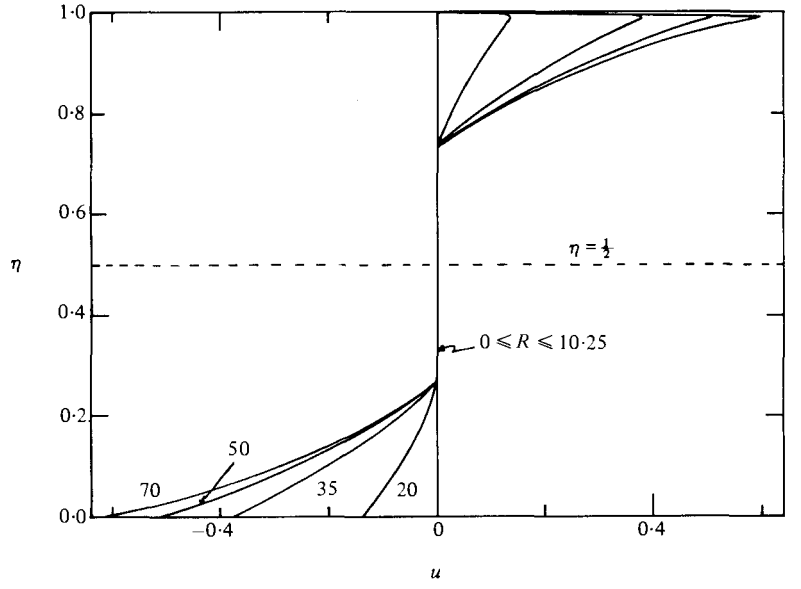

FIGURE 5. The longitudinal-velocity profiles at $x = 0$, i.e. the initial conditions, for the flow in a finite cavity ($h(x) = 1-x^2$). Note that the velocity at $\eta = 1$ was set equal to zero to take into account the presence of the boundary layer at the surface within the collision region. This is not necessary but gives slightly more accurate results near $x = 0$.

over a smaller and smaller region near the origin; until, at $R = 10{\cdot}25$, the two flows agree only at $x = 0$. Beyond this critical Reynolds number, the returning fluid influences the flow everywhere, and a collision region forms at the origin. The onset of the collision region at $R = 10{\cdot}25$ can also be seen in figure 5, where the axial velocity at $x = 0$, i.e. the initial condition, is shown as a function of the Reynolds number.

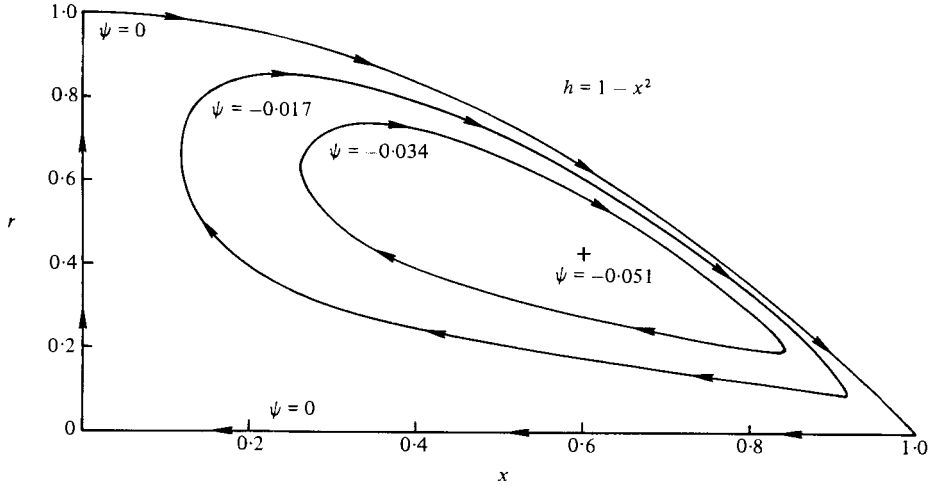

FIGURE 6. Streamline pattern for $R = 10{\cdot}25$, which is typical of those for $0 \leqslant R \leqslant 10{\cdot}25$.

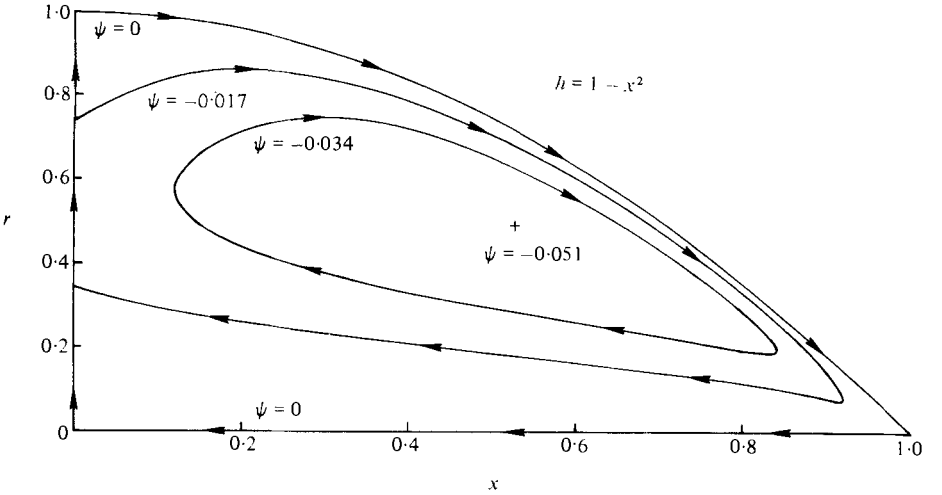

FIGURE 7. Streamline pattern for $R = 35$, which is typical of those for $R > 10{\cdot}25$.

Figures 6 and 7 show how the streamline pattern evolves as the structure of the flow changes with R.

Thus, we have shown that a collision region does indeed appear at $R = 10{\cdot}25$, whose existence enabled us to extend our solutions beyond this critical Reynolds number. Although the mathematical structure of the flow changes fundamentally at $R = 10{\cdot}25$, the actual evolution of the flow with Reynolds number is smooth and continuous (as far as can be deduced from the numerical calculations) as is to be expected for any real physical flow.

The numerical scheme outlined above was found to be computationally efficient and accurate, even to the point of resolving the singularity in (3.1) at $x = 0$. To insure the accuracy of the results, various checks were made on the computations, such as changing the mesh size, as well as using both second-order upwind differences in the x-direction (see Roache 1972) and a fully explicit scheme in time. In fact, a grid size as

small as 11×11 without the exponential stretch gave results within 10 % of those computed with the 26×91 exponentially stretched grid throughout the entire domain, except at $x = 0$, where the extrapolated initial conditions were very poor. Surprisingly, when an intermediate grid size of 26×26 without an exponential stretch was used, the accuracy of the solution near the origin actually decreased. This decrease and then increase in accuracy as the mesh is made finer is a direct result of the singularity in (3.1) at the origin – a very coarse mesh does not notice the singularity, a finer mesh begins to experience its presence but is too coarse to resolve it, and the finest mesh used had no difficulty in resolving the singularity. At the same time, however, second-order upwind differences gave accurate results with the 26×26 grid, but not with the finer 26×91 exponentially stretched grid because, when a very fine mesh was used, the artificial viscosity introduced by the upwind differencing tended to smooth out and incorrectly represent the pressure gradient. Solutions for Reynolds numbers in excess of 70 were not computed because it became increasingly more difficult and time-consuming to reach a steady state. At large Reynolds numbers, the flow over most of the length of the cavity is effectively inviscid, and the numerical scheme we have used is not well suited for calculating the time evolution of an inviscid flow.

As a final part of this section, we would like to show that the appearance of an inviscid collision region at $R = 10{\cdot}25$ is a fundamental property of the accelerating tube-flow problem and is not dependent on the particular geometry we have selected. For this purpose, a shape of $h(x) = 1$, $0 \leqslant x < 1$, and $h(1) = 0$ was chosen which rendered the effective Reynolds number constant over the length of the cavity. For this shape, however, the sudden appearance of a closed end results in a 'singular' region at $x = 1$ in which the fluid carried along by the moving surface is turned around. It is not difficult to see that the flow in this singular region is inviscid (when R is not identically zero), and that its structure is identical to that in the inviscid collision region (cf. § 2). Thus, there are collision regions at both ends of the cavity, and, accordingly, the proper downstream condition for (3.1) is (2.6) rather than (3.5). From a knowledge of the velocity profile for $\eta \geqslant \frac{1}{2}$, we can compute the profile for $\eta \leqslant \frac{1}{2}$, and hence determine how the fluid is to return from the downstream end. Using (2.6) as the condition at both $x = 0$ and $x = 1$ is sufficient to uniquely determine the flow throughout the entire cavity, whereas using (2.6) at $x = 0$ alone without a downstream condition is not.

The numerical computations were performed in the same manner as before, with the exception that both the initial and downstream conditions were found by extrapolation. Since there are now two collision regions, the x-co-ordinate was not exponentially stretched, as this would have removed grid points from the downstream end. Also, a grid size of 26×26 and second-order upwind differences were used in the axial direction because they were found to give sufficiently accurate results with less computing time. No attempt was made to resolve the square-root singularities which are present at both ends, as this would have required excessive computational effort. Even so, the time required to reach a steady state was considerably longer than that previously needed, because both the initial and downstream conditions had to be adjusted in time. The results for the pressure distribution are shown in figure 8, where it is seen that, although the pressure distribution is quite different from that of the previous example, the onset of the collision region still occurs at $R = 10{\cdot}25$. Perhaps not surprisingly, since $h(x) = 1$, the similarity solution represents the flow over a

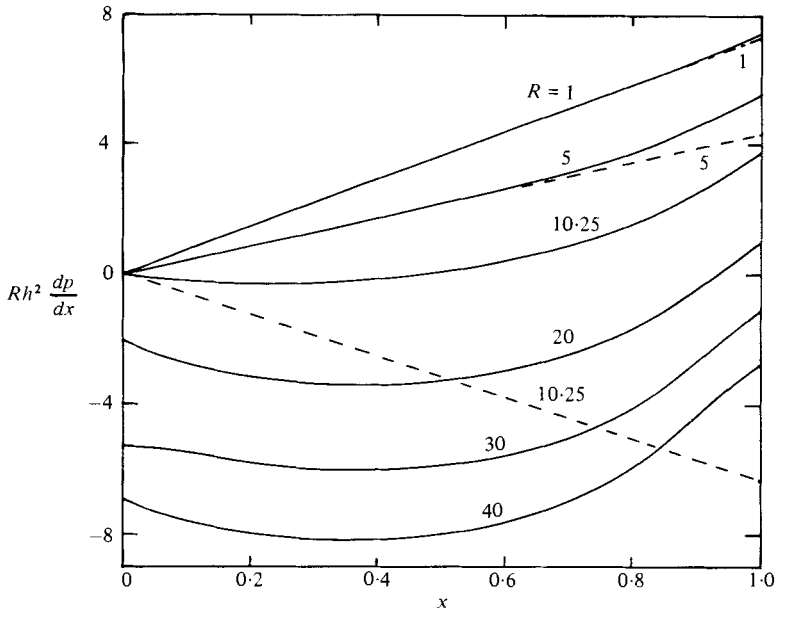

FIGURE 8. Pressure-gradient profiles for the flow in a finite axisymmetric cavity with a sudden end ($h(x) = 1, 0 \leqslant x < 1, h(1) = 0$) at $R = 1, 5, 10{\cdot}25, 20, 30, 40$. The dashed curves correspond to the similarity solution pressure gradients at $R = 1, 5, 10{\cdot}25$.

greater portion of the cavity than was the case when $h = 1-x^2$, but this region of common validity of the two solutions still shrinks to zero as $R \to 10{\cdot}25$.

4. Extension to other flows

We have seen that the flow in a finite-length axisymmetric cavity which is being driven by an accelerating surface velocity undergoes a fundamental change in structure at a critical value of the Reynolds number. As we described in § 1, this transition can be given a simple physical explanation in terms of the effects of the returning fluid, and the results we have obtained are consistent with this explanation and with the inviscid collision region analysis. Furthermore, the values of R at which the collision region first appears and where the similarity solution ceases to exist coincide. (The same was true for the moving-wall boundary-layer problem with reverse flow studied by Klemp & Acrivos (1976).) This may be an accident, however, because there does not seem to be any *a priori* reason why the appearance of a collision region at $x = 0$ should be linked to the non-existence of a similarity solution. Indeed, as the following example serves to indicate, the appearance of a collision region is simply due to the presence of fluid which is returning from downstream.

Consider then the flow in a finite-length, two-dimensional channel – the two-dimensional analogue of the problem we have just considered in § 3. Although a similarity solution to this problem exists for all R (see I), it would indeed be very surprising if the flow in a finite channel were to differ in a fundamental way from that in a finite axisymmetric tube. Thus, using the same shape, $h(x) = 1-x^2$, we repeated the calculations of § 3 for the two-dimensional problem, and the results for the pressure gradient are shown in figure 9. Since upwind differences were used and the x-co-ordinate

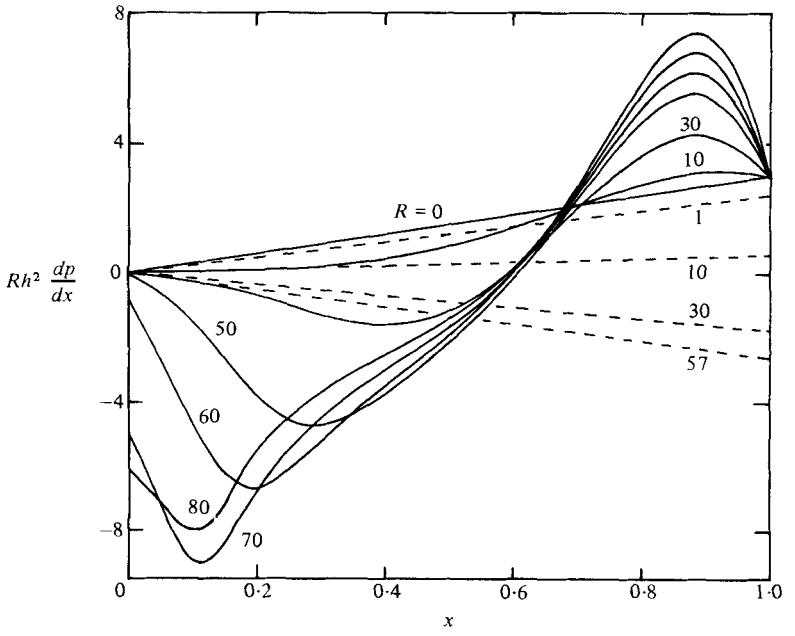

FIGURE 9. Pressure-gradient profiles for the flow in a finite two-dimensional cavity ($h(x) = 1-x^2$) at R = 0, 10, 30, 50, 60, 70, 80. The dashed curves are the similarity solution pressure gradients at R = 1, 10, 30, 57.

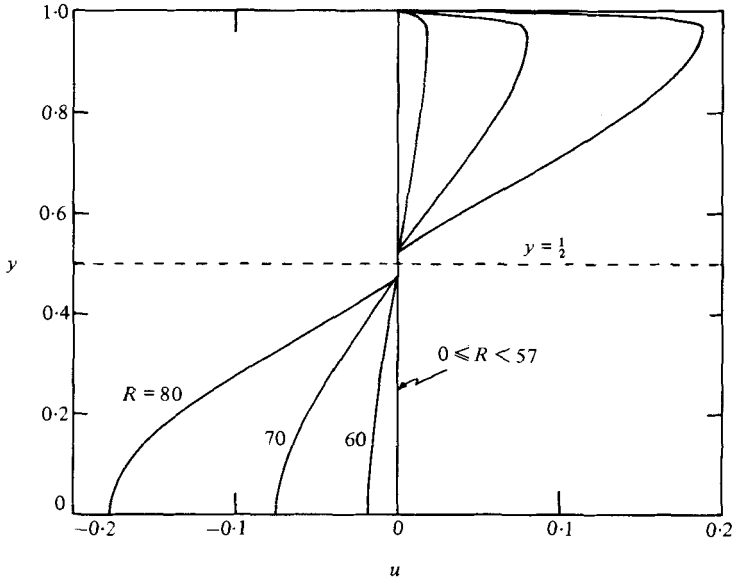

FIGURE 10. The longitudinal-velocity profiles at $x = 0$, i.e. the initial conditions, for the flow in a finite two-dimensional cavity ($h = 1-x^2$). (See note for figure 5.)

was not exponentially stretched, the singularity at the origin does not appear. The computed axial velocity profiles at $x = 0$, shown in figure 10, along with the pressure distributions, clearly demonstrate that an inviscid collision region forms at a critical Reynolds number, even though a similarity solution exists for all R. The exact value of the critical Reynolds number may, of course, depend on the cavity shape; however,

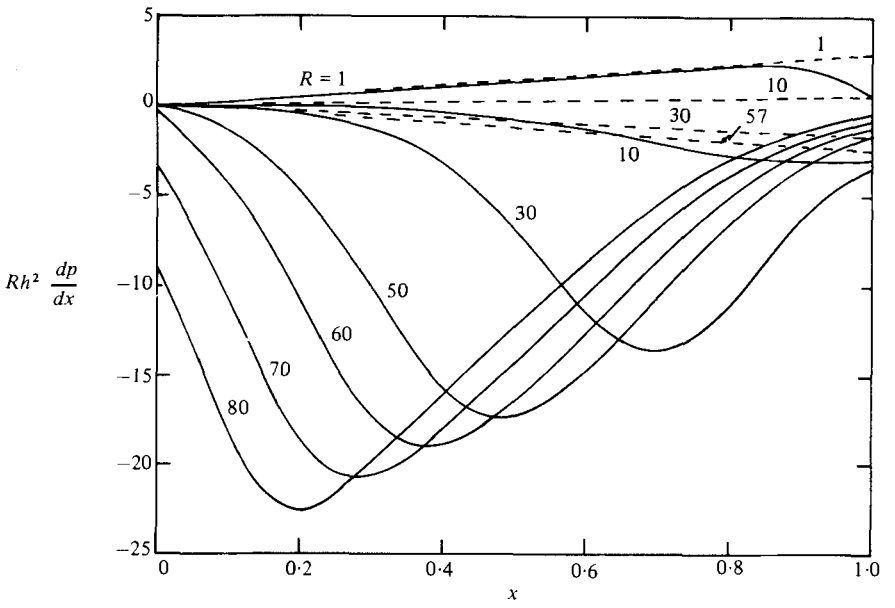

FIGURE 11. Pressure-gradient profiles for the flow in a finite two-dimensional cavity with a sudden end ($h(x) = 1$, $0 \leqslant x < 1$, $h(1) = 0$) at $R = 1, 10, 30, 50, 60, 70, 80$. The dashed curves correspond to the similarity solution pressure gradients at $R = 1, 10, 30, 57$.

when we repeated the calculations for the shape $h(x) = 1$, $0 \leqslant x < 1$, $h(1) = 0$ (see figure 11), both shapes were found to give the same critical Reynolds number of approximately 57.

It should be apparent, by now, that collision regions may arise in many other flows, but, unfortunately, it does not seem possible at present to predict *a priori* whether, in any given problem, a collision region will or will not form.† In the axisymmetric tube flow and the moving-wall boundary-layer flow, the non-existence of the similarity solutions made the need for a collision region almost self-evident, but the same was not true for the channel-flow case. From a practical, or computational, viewpoint, however, this is not an important matter. For we wish to propose that a mathematically and physically correct scheme for integrating the boundary-layer equations through a region of reverse flow is to formulate the initial condition in the manner described in this paper, so that, if a collision region is needed, one will simply emerge.

The fact that the similarity solution no longer represents the flow near the origin of a finite channel when the Reynolds number exceeds 57, even though it appears perfectly reasonable for all values of R, raises an interesting question regarding the applicability of similarity solutions to real flow situations. Of course, several cases have been reported in the literature where similarity solutions either failed to exist or developed singularities within some range of parameter space – cf. Barenblatt & Zel'dovich (1972), Moffatt & Duffy (1980). It has generally been taken for granted, however, that if a similarity solution was found to exist it could be assumed to provide

† A related problem which may help resolve this question concerns the stability of the similarity solution to perturbations in x. A stability analysis can be carried out in much the same way as that for a conventional boundary layer, and it would be of interest to see whether the critical Reynolds numbers determined here could also be predicted by such an analysis.

at least a local representation of the flow. In fact, what our results suggest is that similarity solutions should be viewed with caution because they may have a limited range of applicability — i.e. they may provide a valid representation of a flow over some region of space (even if it is very small) only up to a critical value of the relevant parameter of the problem but, once this critical value is exceeded, the similarity solution may no longer give even an approximate description of a real flow.

This work was supported in part by a grant from the National Science Foundation, ENG 78–17613.

REFERENCES

BARENBLATT, G. I. & ZEL'DOVICH, YA. B. 1972 Self-similar solutions as intermediate asymptotics. *Ann. Rev. Fluid Mech.* **4**, 285–312.

BRADY, J. F. & ACRIVOS, A. 1981 Steady flow in a channel or tube with an accelerating surface velocity. An exact solution to the Navier–Stokes equations with reverse flow. *J. Fluid Mech.* **112**, 127–150.

BRADY, J. F. & ACRIVOS, A. 1982 The deformation and breakup of a slender drop in extensional flow: inertial effects. *J. Fluid Mech.* **115**, 443–451.

KLEMP, J. B. & ACRIVOS, A. 1972 A method for integrating the boundary-layer equations through a region of reverse flow. *J. Fluid Mech.* **53**, 177–191.

KLEMP, J. B. & ACRIVOS, A. 1976 A moving-wall boundary layer with reverse flow. *J. Fluid Mech.* **76**, 363–381.

MOFFATT, H. K. & DUFFY, B. R. 1980 Local similarity solutions and their limitations. *J. Fluid Mech.* **96**, 299–313.

ROACHE, P. J. 1972 *Computational Fluid Dynamics*, p. 73. Hermosa.

VAN DYKE, M. 1970 Entry flow in a channel. *J. Fluid Mech.* **44**, 813–823.